

Modeling Respiratory Movement Signals During Central and Obstructive Sleep Apnea Events Using Electrocardiogram

AHSAN H. KHANDOKER and MARIMUTHU PALANISWAMI

Department of Electrical & Electronic Engineering, The University of Melbourne, Parkville, VIC 3010, Australia

(Received 15 July 2010; accepted 12 October 2010; published online 23 October 2010)

Associate Editor John H. Linehan oversaw the review of this article.

Abstract—Obstructive sleep apnea (OSA) causes a pause in airflow with continuing breathing effort. In contrast, central sleep apnea (CSA) event is not accompanied with breathing effort. CSA is recognized when respiratory effort falls below 15% of pre-event peak-to-peak amplitude of the respiratory effort. The aim of this study is to investigate whether a combination of respiratory sinus arrhythmia (RSA), ECG-derived respiration (EDR) from R-wave amplitudes and wavelet-based features of ECG signals during OSA and CSA can act as surrogate of changes in thoracic movement signal measured by respiratory inductance plethysmography (RIP). Therefore, RIP and ECG signals during 250 pre-scored OSA and 150 pre-scored CSA events, and 10 s preceding the events were collected from 17 patients. RSA, EDR, and wavelet decomposition of ECG signals at level 9 (0.15–0.32 Hz) were used as input to the support vector regression (SVR) model to recognize the RIP signals and classify OSA from CSA. Using cross-validation test, an optimal SVR (radial basis function kernel; $C = 2^8$ and $\epsilon = 2^{-2}$ where C is the coefficient for trade-off between empirical and structural risk and ϵ is the width of ϵ -insensitive region) showed that it correctly recognized 243/250 OSA and 139/150 CSA events (95.5% detection accuracy). Independent test was performed on 80 OSA and 80 CSA events from 12 patients. The independent test accuracies of OSA and CSA detections were found to be 92.5 and 95.0%, respectively. Results suggest superior performance of SVR using ECG as the surrogate in recognizing the reduction of respiratory movement during OSA and CSA. Results also indicate that ECG-based SVR model could act as a potential surrogate signal of respiratory movement during sleep-disordered breathing.

Keywords—Central sleep apnea, Obstructive sleep apnea, Respiratory movements, Support vector regression, Electrocardiogram.

Address correspondence to Ahsan H. Khandoker, Department of Electrical & Electronic Engineering, The University of Melbourne, Parkville, VIC 3010, Australia. Electronic mail: ahsank@unimelb.edu.au

INTRODUCTION

The respiratory pump consists of not only the respiratory muscles, but also the structure of rib cage and abdomen controlled by the brain, spinal cord, and the peripheral nerves. The control mechanism of the respiratory pump is different from that of the upper airway during sleep.²⁰ Obstructive sleep apnea (OSA) is a temporary closure of the upper airway during sleep when air is prevented from entering lungs. The onset of each OSA is associated with inspiratory efforts against a closed airway, which increase parasympathetic activity leading to a bradycardia, but as the physiological stress builds up during the apnea, the sympathetic activity predominates. This peaks shortly after the moment of arousal at which time there is systemic vasoconstriction, hypertension, and a tachycardia. Termination of OSA requires arousal from a deeper-to-lighter stage of sleep or wakefulness.²⁰

An observation during central sleep apnea (CSA), on the other hand, reveals an absence of respiratory movements which differentiate these apneas from OSA. These observations can be confirmed by sleep studies in which abdominal and chest wall movement recordings are combined with airflow and oximetry. CSA is recognized when respiratory effort falls below 15% of pre-event peak-to-peak amplitude of the respiratory effort. The arousals are less frequent than in OSA because of the absence of any increased inspiratory effort as an arousal stimulus. During CSA, the P_{CO_2} gradually rises and when it reaches the apnoeic threshold, a period of hyperventilation then begins to lower the P_{CO_2} again.²⁰

Approximately, 50% of heart failure patients experience sleep-disordered breathing,³ with either central sleep apnea (CSA) or obstructive sleep apnea (OSA) usually predominating, but both are often present. Optimizing the treatment for congestive heart failure is

the first step of CSA treatment. Various forms of continuous positive airways pressure (CPAP) are used for CSA treatment. The use of CPAP has been shown to improve cardiac function and quality of life, and lessen the need for transplantation. However, it is important to distinguish CSA from OSA events because different types of sleep apneas may require different treatment approaches. Also, this distinction is important to understand the pathophysiological mechanisms of different types of apnea. Different algorithms on cheaper ambulatory ECG monitoring technology for the detection of OSA have recently been reported.^{15,17,18} However, the reported methods assess whether the ECG could detect OSA during each minute of the recording and hence cannot detect the actual events. We have recently developed a model for detection of individual apnea events and types (apnea/hypopnea),¹⁰ but that model could not distinguish OSA from CSA events.

At present, the clinical technique for respiratory monitoring during sleep is the use of two respiratory inductance plethysmography (RIP) measurements (rib-cage and abdominal), which can be used with reasonable agreement with those of the standard reference methods of measurement for respiratory effort-related arousals (RERA), central hypopnea–apnea, and Cheyne–Stokes respiration (CSR) associated with central sleep apnea CSR-CSA.¹ For OSA and CSA screening using RIP signals, patients are referred to a sleep clinic for an overnight polysomnographic (PSG) study. This process is expensive, needing dedicated systems and attendant personnel. It is not suitable for mass screening; waiting periods are long, and rural areas lack sleep clinics; therefore, vast majority remains undiagnosed for long periods. Other disadvantage of laboratory PSG is the artificial sleep environment (which may affect how the patient sleeps). Fast, clinical or domiciliary, diagnostics would be hugely beneficial in terms of early detection and cost. This has recently been acknowledged by the US Center of Medicare Services who now allow for home diagnosis reimbursement. There is evidence that for people with a high probability for sleep apnea, use of facility-based PSG does not result in better outcomes over an ambulatory approach in terms of diagnosis and CPAP titration.²² The American Sleep Disorders Association classified the different monitors that have been used in sleep studies into four categories, depending on which channels they record and evaluate.⁷ Among them, type IV may include monitors that record one or two bioparameters. For example, ECG-based apnea event detection algorithm as proposed by our previous studies^{10,11} fit into type IV monitor. In order to make the best use of the ECG-based apnea classification device, modeling surrogate respiratory signals using

ECG signals could be useful for apnea types classification in the situation of unattended home setting.

The phenomenon of respiratory modulation of the chest ECG has already been widely noted, and there are a number of studies in the literature reporting algorithms for estimation of respiratory signals from the ECG.^{12,13,16,21} ECG are reported to be modulated by respiration mainly in two different ways: (1) respiratory sinus arrhythmia (RSA) using modulations of beat-to-beat heart rate caused by respiration, or (2) ECG-derived respiration (EDR) using variations of the beat morphology, especially of the R-peak, induced by respiration.^{11–13,16,21}

In this study, we use discrete wavelet transform of ECG signals to extract the respiratory-related component and combine with RSA and EDR using support vector regression (SVR). The primary objective is to determine whether surrogate respiratory signal extracted from ECG signal surrounding OSA and CSA can correlate with respiratory signal measured by RIP. A secondary objective is to determine whether changes in mean peak-to-peak amplitude of the surrogate respiratory signal can discriminate CSA from OSA.

METHODS

Subjects and Sleep Studies

In total, 17 and 12 PSG recordings were used to develop and validate our classification algorithms, respectively. PSGs were collected from the database of the Institute of sleep and breathing, Austin Hospital, Melbourne, Australia (a collaborative partner with the University of Melbourne). The research protocol was approved by Austin Ethics in Human Research Committee (H2008/03252). Brief descriptions of the databases are as follows. The PSG recordings of the training set of 17 sleep apnea patients [(mean \pm SD) age 54 ± 5 years, body mass index (BMI) 31 ± 2 kg/m², 10 men and 7 women], and a test set of 12 sleep apnea patients [(mean \pm SD) age 51 ± 2 years, body mass index (BMI) 30 ± 5 kg/m², 10 men and 2 women] were analyzed by Pro-Fusion software version 3 (Compu-medics Pty Melbourne, Australia). Each PSG study included electroencephalogram (channels C3–A2 and C4–A1), left- and right electrooculograms, leg movements, body positions, thoracic and abdominal wall expansion (using by RIP), oronasal airflow (by nasal pressure), arterial oxygen saturation SaO₂ (by pulse oximetry), and ECG (sampling frequency = 250 Hz with a resolution of 16 bits/sample). All the subjects were free of any cardiac history. Diagnosis was based on clinical symptoms and PSG outcomes. Respiratory events were scored by an expert using criteria proposed by the AASM.¹ Only full apnea events were considered

in this study excluding hypopneas. There has been no personal bias in the event selection process. 250 pre-scored OSA events and 150 pre-scored CSA events were randomly selected from 10 patients and 7 patients, respectively, to develop the algorithm. In order to validate the algorithm, 80 OSA and 80 CSA events were taken from 12 patients.

Scoring Method

The OSA event was scored as 80–100% reduction of oronasal airflow for >10 s using the criteria that a reduction of 50–85% from peak-to-peak (mean positive to mean negative) amplitude of RIP signals (sampling frequency = 32 Hz) must be in both the thoracic and abdominal movement channels (which were recorded on separate channels for this study). Events were followed by either an oxygen desaturation of $\geq 3\%$ or an arousal.

The CSA event, on the other hand, was scored as the absence of oronasal airflow for >10 s in using the criteria that a reduction of >85% from peak-to-peak (mean positive-to-mean negative) amplitude of RIP signals must be in both the thoracic and abdominal movement channels (which were recorded on separate channels for this study). Events were followed by either an oxygen desaturation of $\geq 3\%$ or an arousal.

The range of apnea–hypopnea index (AHI) of patients was 12.5–85.45. Figure 1 shows an example of a PSG recording (5 min) in a patient with OSA and CSA events (AHI = 48.5 events/h).

ECG Clips

A total of 250 (training set) and 80 (test set) simultaneous ECG and RIP (thoracic movement) signal clips of 20-s duration (10-s preceding and 10-s following the onset of OSA events) collected from 330 pre-scored OSA events were selected. Similarly, 150 (training set) and 80 (test set) simultaneous ECG and RIP signal clips (10-s preceding and 10-s following the onset of CSA events) collected from 230 pre-scored CSA events with/without arousals were extracted for analysis in this study.

Derivation of EDR Signals Through RSA, EDR, and Wavelet-EDR from Wavelet-Decomposed ECG Signals

RSA

The sampling frequency of the ECG signal was 250 Hz. In order to calculate R–R interval with an error in accuracy of less than one beat per min, ECG signal was resampled using cubic spline interpolation at a sampling frequency of 4000 Hz.⁹

EDR

The method for calculation of an EDR is through interpolation of the amplitude values of the R-peaks of the ECG. A highpass (0.05 Hz cutoff frequency) FIR filter was used to remove the baseline wandering from that caused in R-peak amplitudes by respiration.

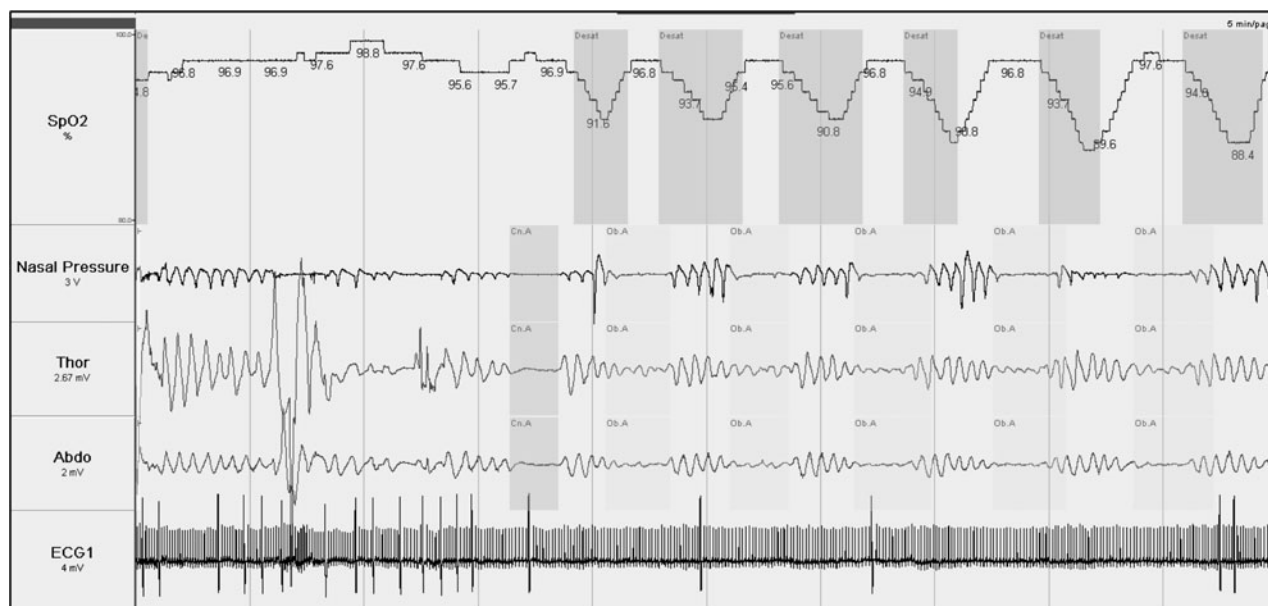


FIGURE 1. Example of digital recordings (5 min) in a patient with obstructive and central sleep apnea (AHI = 48.5). The uppermost trace is SpO2 (%; pulse oximeter); second, nasal pressure; third, thoracic movement signals; Fourth, abdominal movement signals, and the lowermost is that of ECG signals (Lead I); CnA = Central apnea; ObA = Obstructive apnea.

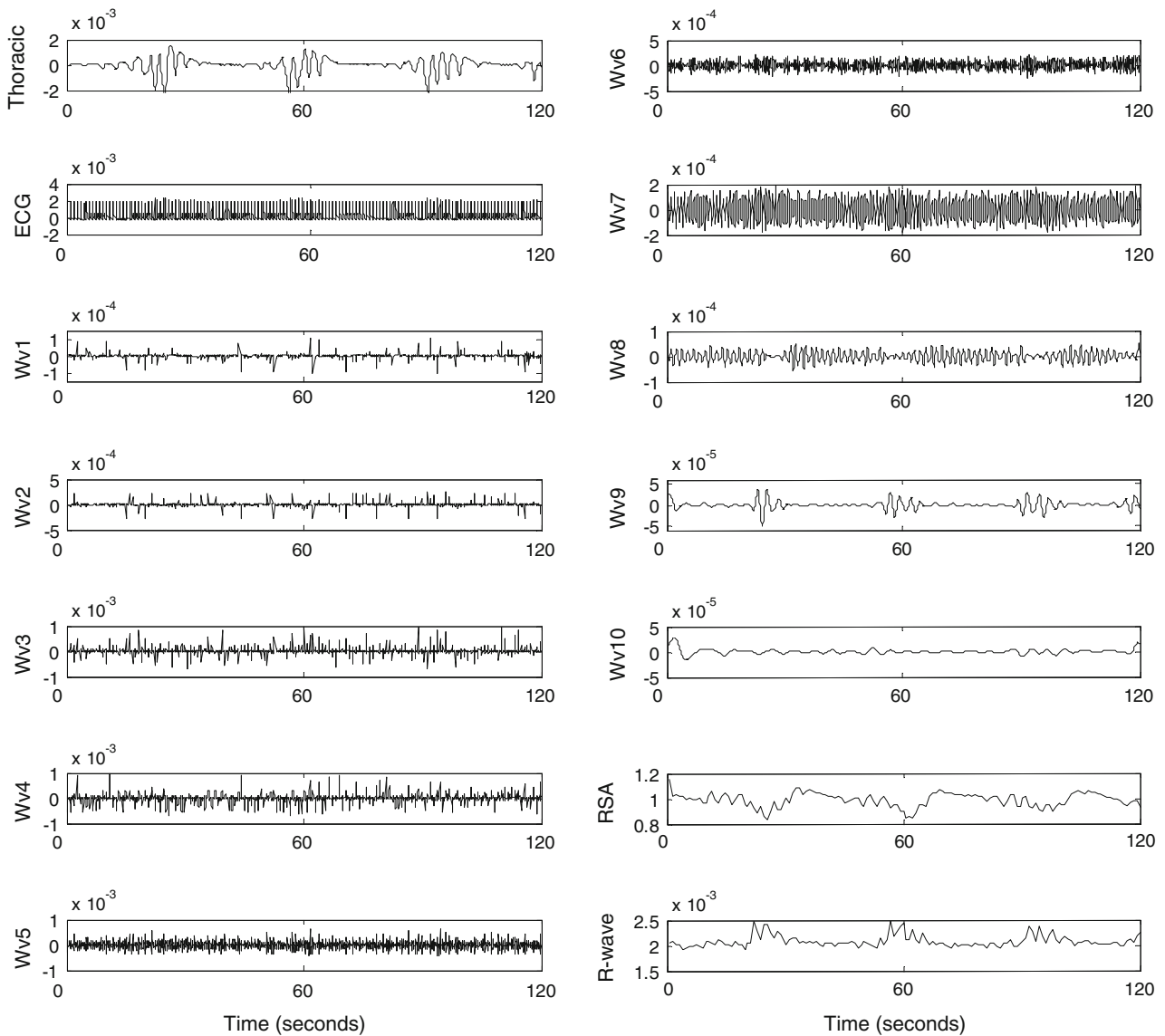


FIGURE 2. Two-minute recording of thoracic movement signal (V), ECG signals and its reconstructed wavelet-detailed decomposition up to level 10, RSA, and EDR of a sleep apnea patient (AHI = 48.5) during four central apnea breathing episodes. RSA, EDR, and wavelet-decomposed ECG signals were resampled using cubic spline interpolation to make 3840 samples.

Wavelet-EDR

A discrete wavelet transform of 20-s ECG clip was used to decompose the signal into a set of approximate and detailed coefficients of level up to 10. Reconstructed detailed coefficients up to level 10 were computed. A symlet wavelet with order 8 was chosen as the mother wavelet for decomposition. Wavelet decomposition of ECG signals (during central apnea breathing episodes), RSA, and EDR of a sleep apnea patient (AHI = 48.5) are illustrated in Fig. 2. Reconstructed decomposition level 9 (i.e., 0.15–0.32 Hz) was chosen as the wavelet-EDR feature because the range of breathing frequency overlaps with that range.

In this study, SVR model was considered to distinguish CSA from OSA events from a combination (RSA, EDR, and wavelet-EDR) of ECG features. In order to match the number of samples in RIP as the target signal (total 640 samples in 20 s with a sampling frequency, 32 Hz), RSA, EDR and wavelet-EDR signals were resampled using cubic spline interpolation (MATLAB) to produce 640 samples.

SVR

Support Vector Machines (SVMs) are a relatively new class of learning machines that have evolved from

the concepts of structural risk minimization (SRM) (in the pattern recognition case) and regularization theory (in the regression case).²³ The major difference between SVMs and many other Neural Network (NN) approaches is that instead of tackling problems using the traditional empirical risk minimization (ERM) method, SVMs use the concept of regularized ERM. This has enabled researchers to use SVMs with potentially high capabilities on smaller datasets without running into the usual difficulties of overfitting and poor generalization performance. Geometrically, the basis of SVM theory is to nonlinearly map the input data into some (possibly infinite dimensional) feature space where the problem may be treated as a linear one. In particular, when tackling regression problems using SVMs, the output is a linear function of position in feature space.

ε -SV Regression

The standard SV regression problem (ε -SV Regression) is formulated as follows.

Suppose we are given a training set ($x_i = \text{input}; z_i = \text{target}$):

$$\begin{aligned} \Theta &= \{(x_1, z_1), (x_2, z_2), \dots, (x_N, z_N)\} \\ x_i &\in \mathbb{R}^{d_L} \\ z_i &\in \mathbb{R} \end{aligned}$$

where d_L is the dimension of x_i , which is assumed to have been generated based on some unknown but well-defined map:

$$\hat{g}: \mathbb{R}^{d_L} \rightarrow \mathbb{R}$$

$$z_i = \hat{g}(x) + \text{noise}$$

so that

$$x_i = \hat{x}_i + \text{noise}$$

Let us define a set of functions (implicitly, as will be seen later) $\phi_j: \mathbb{R}^{d_L} \rightarrow \mathbb{R}$, $1 \leq j \leq d_H$, which collectively makes up a map from input space to feature space, namely, $\phi_j: \mathbb{R}^{d_L} \rightarrow \mathbb{R}^{d_H}$, where d_H is the dimension of x_i in the feature space ϕ and

$$\phi(x) = \begin{bmatrix} \phi_1(x) \\ \phi_2(x) \\ \vdots \\ \phi_{d_H}(x) \end{bmatrix}$$

Using the function, $\phi_j: \mathbb{R}^{d_L} \rightarrow \mathbb{R}$, $1 \leq j \leq d_H$, we aim to find a nonlinear approximation to $\hat{g}: g(x) = w^T \phi(x) + b$ which is a linear function of position in

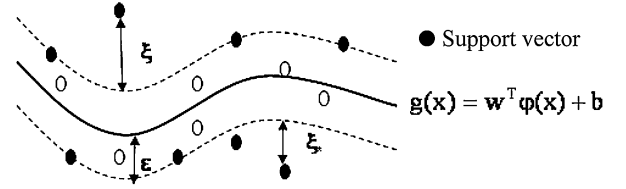


FIGURE 3. Support vector regression (SVR) and its parameters (ε , ξ , ξ^*). ε is a precision parameter representing the radius of the tube located around the regression function $g(x)$ (the broken lines). The region enclosed by the tube is known as “ ε -insensitive zone” since the loss function assumes a zero value in this region and does not penalize the prediction errors with magnitudes smaller than ε . Two positive slack variables, ξ and ξ^* , can be used to measure the deviation from the boundaries of the ε -insensitive zone. They represent the distance from actual values to the corresponding boundary values of ε -insensitive zone.

feature space. The usual ε -SVR method of selecting w and b is to minimize the regularized risk functional:

$$\begin{aligned} \min_{w, b, \xi, \xi^*} R(w, b, \xi, \xi^*) &= \frac{1}{2} w^T w + \frac{C}{N} \mathbf{1}^T \xi + \frac{C}{N} \mathbf{1}^T \xi^* \\ \text{Such that :} & \\ (w^T \phi(x_i) + b) &\geq z_i - \varepsilon - \xi_i \\ -(w^T \phi(x_i) + b) &\geq -z_i - \varepsilon - \xi_i^* \\ \xi, \xi^* &\geq 0 \end{aligned} \quad (1)$$

where $\frac{1}{2} w^T w$ characterizes the complexity of the model (the larger the $\frac{1}{2} w^T w$, the larger the gradient of $g(x)$ in feature space, and hence the more the $g(x)$ may vary for a given variation in input, x), and $\frac{1}{N} \mathbf{1}^T \xi + \frac{1}{N} \mathbf{1}^T \xi^*$ characterizes the empirical risk associated with it. A schematic representation of the SVR using ε -insensitive loss function is illustrated in Fig. 3.

The constant $C > 0$ controls the trade-off between empirical risk minimization (and potential over-fitting) if C is large and complexity minimization (and potential under-fitting) if C is small.

The constant $\varepsilon > 0$ term in (1) is included to give the model a degree of noise insensitivity. Essentially, as long as $z_i - \varepsilon \leq g(x_i) \leq z_i + \varepsilon$, $\xi_i^* = \xi_i = 0$, and so there will be no empirical risk associated with small perturbations (specifically, those perturbations which leave the point lying inside the ε tube), giving the risk functional a degree of noise immunity (assuming that ε is well matched to the noise present in the training data).

The function $K(x_i, x_j) = \phi(x_i)^T \phi(x_j)$ is called the kernel function. It is not difficult to show that our approximation function $g(x)$ may be written in terms of the kernel function:

$$g(y) = \sum_i (\alpha_i - \alpha_i^*) K(x_i, y) + b \quad (2)$$

Note that the feature map functions $\phi_j: \mathbb{R}^{d_L} \rightarrow \mathbb{R}$ are hidden by the kernel function. It is well known that for

any symmetric function $K : \mathbb{R}^{d_L} \times \mathbb{R}^{d_L} \rightarrow \mathbb{R}$ satisfying Mercer's condition,⁵ there exists an associated set of feature maps $\phi_j : \mathbb{R}^{d_L} \rightarrow \mathbb{R}$ (although calculating what these maps are may not be a trivial exercise). Indeed, we may start with such a kernel function and, with no knowledge of ϕ at all (except that it exists), optimize and use a SV regressor. Feature space remains entirely hidden throughout the process. Linear kernel defined as $K(x_i, x_j) = x_i \cdot x_j$ and Radial basis function (RBF) defined as $K(x_i, x_j) = \exp\left(\frac{-\|x_i - x_j\|^2}{2\sigma^2}\right)$ were used in this study as the kernel function where σ denotes the width of the RBF. Cherkassky and Ma⁴ pointed out that for multivariate d-dimensional problems, the RBF width parameter σ is set as $\sigma^d = 0.1-0.5$, where d is number of input variables. In this study, $\sigma = 0.7$ is used for all the experiments.

Training and Testing the Linear SVR

A tenfold cross-validation scheme was adopted to evaluate the generalization ability of the SVR as a classifier for OSA and CSA. In this scheme, a data set of 400 events (250 OSA and 150 CSA) set was randomly divided into 40 subsets, of which 10 events were used for testing and the remaining 390 events were used to train SVR parameters. There was no fixed proportion of OSA/CSA maintained during cross validation. This was repeated for other subsets so that all subsets were used as the cross-validation test sample. Only linear and RBF kernel were tested in this study. All SVM architectures were trained and tested on the MATLAB SVM toolbox.⁸

RESULTS

Maximum mean cross-validation accuracy was found to be 95.5% ($\pm 3.8\%$) with $C = 2^8$; $\varepsilon = 2^{-2}$ using RBF kernel, where C is the coefficient for trade-off between empirical and structural risk, and ε is the width of ε -insensitive region. The best feature subset was the combination of the wavelet decomposition level (level 9; 0.15–0.32 Hz) of ECG, RSA, and EDR (R-wave amplitude of ECG signals).

A grid search proposed by Bao and Liu² was used in this study for setting parameters of C and ε . To reduce the computational burden, a finer grid search on that region was conducted only after identifying a better region on the grid. We first used a coarse grid search using linear kernel and found the best (C, ε) as $(2^6, 2^{-2})$ with tenfold cross-validation accuracy 90.4% on 50 OSA and 50 CSA events. After the best (C, ε) was found, the model was trained with whole training set (400 events) again to generate the final classifier. The

TABLE 1. SVR model parameter selection.

Kernel	ε	C	Accuracy (%)
Linear	2^{-1}	2^{-2}	79.9
		2^{-1}	83.2
		2^2	84.5
	2^{-2}	2^4	88.9
		2^6	90.4
		2^8	88.9
		2^{10}	87.6
	2^{-4}	2^{12}	86.9
		2^{14}	83.8
		2^6	91.2
RBF ($\sigma = 0.7$)	2^{-2}	2^8	95.5
		2^{10}	94.3

parameter set of C and ε which generated the maximum OSA/CSA classification accuracy (95.5%) was considered as the best parameter set (Table 1). Test Studies (80 OSA and 80 CSA events) were used to provide an independent test performance assessment of our model.

Figure 4 shows an example of RIP (thoracic movement) signal and SVR-based surrogate respiratory signal of 20-s duration (10-s preceding and 10-s following the onset of OSA events) from a pre-scored OSA event. Similarly, Fig. 5 shows RIP (thoracic movement) signal and SVR-based surrogate respiratory signal of (10-s preceding and 10-s following the onset of CSA events) from a pre-scored CSA event. A schematic flow representation of the proposed recognition system for OSA and CSA has been shown in Fig. 6.

Figure 7 shows the correlations of percentage (%) drop in thoracic and surrogate respiratory signals from 10 s preceding the events for 250 OSA and 150 CSA events. Significant correlations ($r = 0.76$; $p < 0.01$ for OSA and $r = 0.54$; $p < 0.01$) were found between reductions in thoracic and that in surrogate respiratory signals. Using surrogate respiratory signals, 243 OSA and 139 CSA events (as cross-validation training set) are correctly recognized. The threshold was set at 85% drop from the preceding thoracic movement. An independent test was carried out on 80 OSA and 80 CSA events collected from 12 patients (Table 2). Test results showed that 74 out of 80 OSA events and 76 out of 80 CSA events have correctly been identified by the SVR model.

The Bland–Altman plot is the preferred method for assessing whether an established and a new measurement technique agree. It shows the paired difference between two observations on each subject against the mean of these two observations Figs. 8a and 8b show Bland–Altman-plots for OSA and CSA events, respectively. Percentage (%) drop in surrogate respiratory signals during OSA events were unbiased, and it overestimated the % drop in thoracic signals by less than 1% (mean bias = +0.82%; +2SD: +13.62%, -2SD: -11.97%). Percentage (%) drop in thoracic

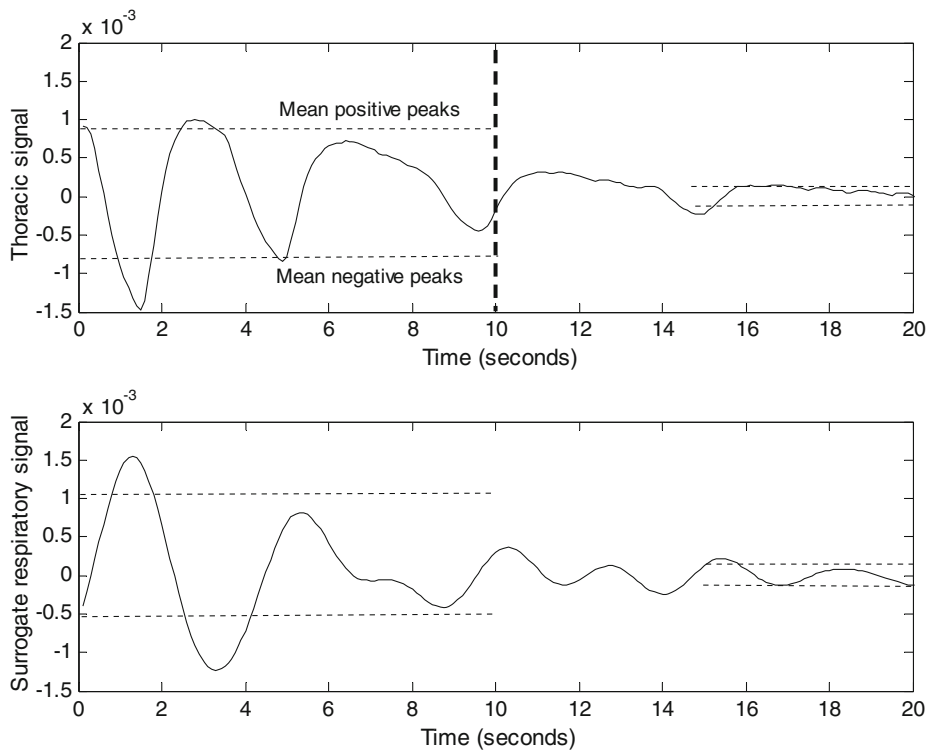


FIGURE 4. An example of thoracic signal and ECG-based surrogate respiratory signal 10 s preceding and 10 s after the start of an OSA event. Thick dashed line represents the start of the pre-scored OSA event.

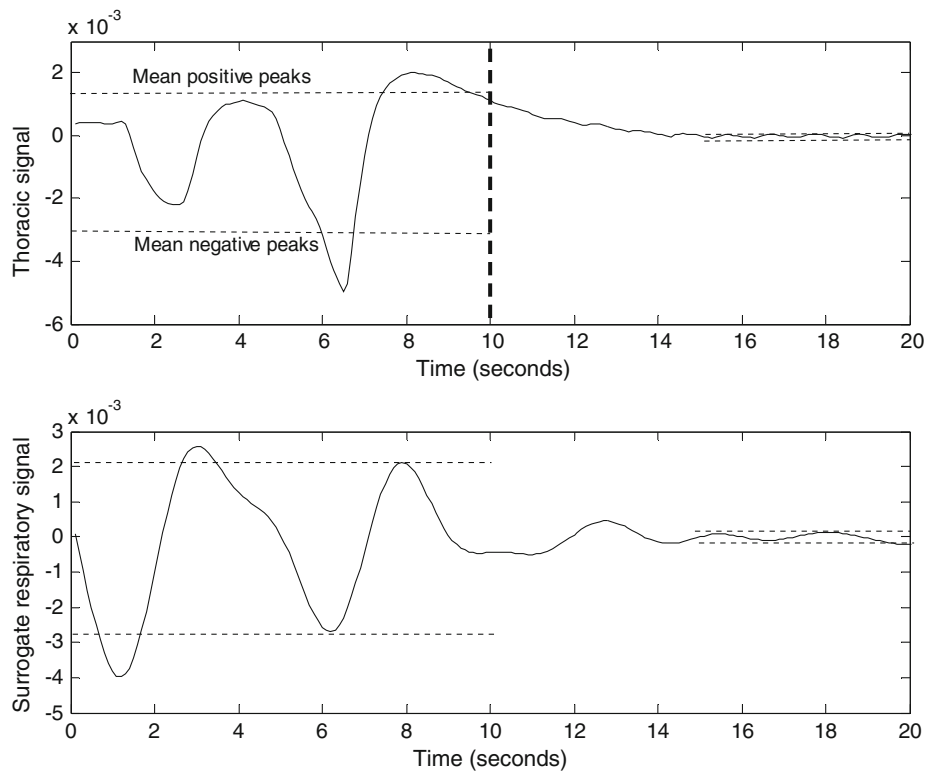


FIGURE 5. An example of thoracic signal and ECG-based surrogate respiratory signal 10 s preceding and 10 s after the start of a CSA event. Thick dashed line represents the start of the pre-scored CSA event.

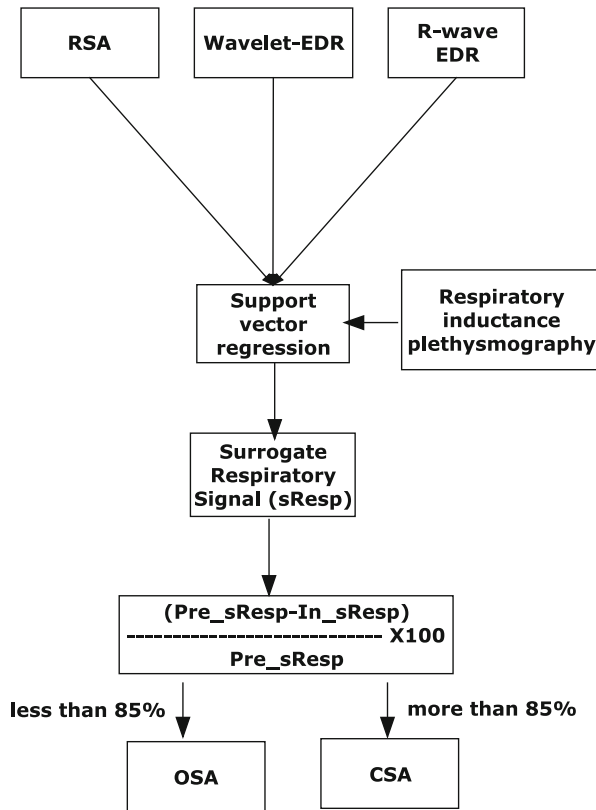


FIGURE 6. Schematic representation of training the proposed diagnostic system for recognizing OSA and CSA-based on ECG signals. Respiratory inductance plethysmogram signal was used as target signal for training. Pre_sResp = mean peak-to-peak amplitude of 10-s sResp preceding an OSA or CSA event. In_sResp = mean peak-to-peak amplitude of 10-s following the onset of the OSA or CSA event.

signals during CSA events was overestimated by less than 2% mean bias = +1.23%; +2SD: + 7.68%, -2SD: -5.23%). Visual inspection of Fig. 8b shows that the surrogate respiratory signal tended to estimate lower percentage drop in thoracic signal unbiased but it tended to under estimate higher percentage drop.

In order to show the comparative performance, OSA/CSA classification performances (overall accuracy, sensitivity, and specificity) on independent test set (80 OSA and 80 CSA events) using (1) RSA, (2) EDR, and (3) a combination of RSA, EDR, and wavelet-EDR features by SVR are summarized in Table 3. The results show that SVR-based OSA/CSA classifier outperforms the RSA or EDR or wavelet-EDR-based classification. However, wavelet-EDR-based classification performance is better than RSA or EDR-based classification as shown in Table 3.

DISCUSSION

SVR which is a powerful regression tool, has been applied to model respiratory effort signal during sleep

apnea events to classify OSA and CSA events for the first time in this study. Despite the rapid advances in the understanding of the nature of sleep-related breathing disorders over the past few years, sleep apneas still often remain unrecognized and untreated. The study results indicate a correlation between changes in amplitudes of surrogate respiratory signal obtained from ECG and the amplitudes of breathing movement during OSA and CSA. Results also showed that SVR with an optimal parameter set correctly recognized 243/250 OSA and 139/150 CSA events (95.5% recognition) in the cross-validation training set. Independent test results showed 93.75% classification accuracy on 160 events (80 OSA and 80 CSA).

EDR

The morphology and amplitude of the ECG change with respiration (i.e., EDR) because of the motion of the electrodes and due to the changing intra-thoracic impedance. However, the performance of the EDR is affected by the position of the electrical axis of the heart. For example, if the ECG lead and electrical axis of the heart are perpendicular, the project of ECG variations caused by respiration also decrease. Also, airway obstruction modulation depth on the ECG varies from patient to patient and throughout the night with changes in postural position as reported by a previous study.¹⁴ Moody *et al.*¹³ described a method of calculating EDR by measuring mean axis direction in two roughly orthogonal leads. No quantitative comparison of their technique with reference methods was provided, and the effect of different body position was not investigated. The assessment of the respiratory signal by the RSA technique has been especially suitable to derive the respiratory rate from ECG recordings.⁶ However, unreliable respiratory patterns are observed in RSA and EDR in the presence of premature ventricular contract (PVC) beat; therefore, the PVC beat needs to be excluded.

Combining wavelet-based EDR with RSA and R-wave amplitude-based EDR in our study appears capable of providing useful discriminative information about respiration during OSA and CSA (Table 3). An important aspect of our study is that postural position appears to have only a small effect on the wavelet-EDR estimates because wavelet decomposition excludes the body position's influence on ECG. Therefore, it can be inferred that single-lead ECG technique may be able to sufficiently identify major respiratory events such as OSA and CSA. If ECG signals get corrupted or disturbed, then SVR cannot derive surrogate respiratory movement signals. The artifacts that may corrupt ECG signals include body movements, improper attachment of ECG electrodes on chest, etc.

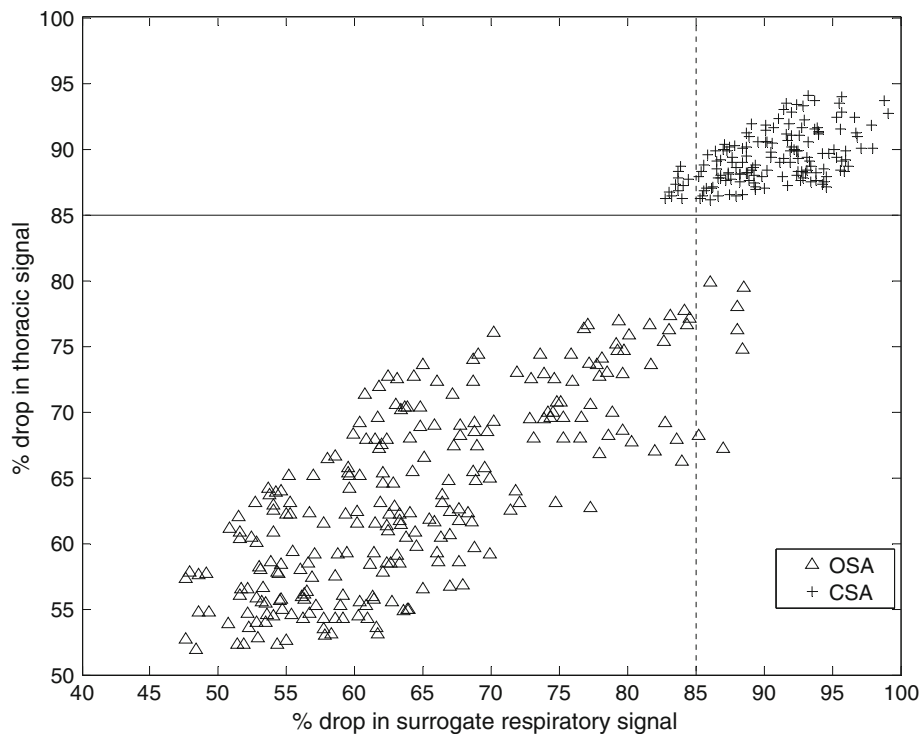


FIGURE 7. Percentage (%) drops in thoracic and surrogate respiratory signals from 10 s preceding the events. A total of 250 OSA and 150 CSA events are shown. Using surrogate respiratory signals, 243 OSA and 139 CSA events are correctly recognized. 85% drop from the preceding thoracic movement was considered as the threshold.

TABLE 2. Comparisons on original OSA/CSA events and the model-based events of 17 patients in the training set and 12 patients in the independent test set.

	Number of patients	Original		Model		Classification accuracy (%)	OSA detection (%)	CSA detection (%)
		OSA	CSA	OSA	CSA			
Training set	17	250	150	243	139	95.50	97.20	92.66
Test set	12	80	80	74	76	93.75	92.50	95.0

Phase differences between thoracic signal and ECG-derived surrogate respiratory signal (as shown in Figs. 4, 5) indicate either paradoxical breathing (out-of-phase movements of the thorax and abdominal cavities), or at least phase-shifted movements (the peaks of the indicators of the chest and abdomen do not line up exactly). Often, the beginning of an obstructive apnea is the peak of the previous in-phase, large breath. Similarly, the ending of an obstructive apnea is often the beginning of the next in-phase, large breath. However, an obstructive apnea does not always have to have paradoxical breathing associated with it. Sometimes, the movement channels indicate in-phase breathing. This is because not enough negative airway pressure has developed to partially compress the chest cavity.¹ The thoraco-abdominal separation influences flow and pressure in both superior and inferior vena cava.²⁴

Regression Model

Model parameters such as C and ϵ are selected by users based on *a priori* knowledge and/or user expertise.¹⁹ Obviously, this approach is not appropriate for non-expert users. It is well known that SVR generalization performance (estimation accuracy) depends on a good setting of meta-parameters parameters C , ϵ and the kernel parameters. The problem of selection of the optimal parameter is further complicated by the fact that SVR model complexity (and hence its generalization performance) depends on all three parameters. Existing software implementations of SVR usually treat SVR meta-parameters as user-defined inputs. In this article we focused on the choice of C and ϵ , rather than on selecting the kernel function. OSA/CSA classification accuracy on cross-validation data set rather than root mean squared error (RMSE) was considered

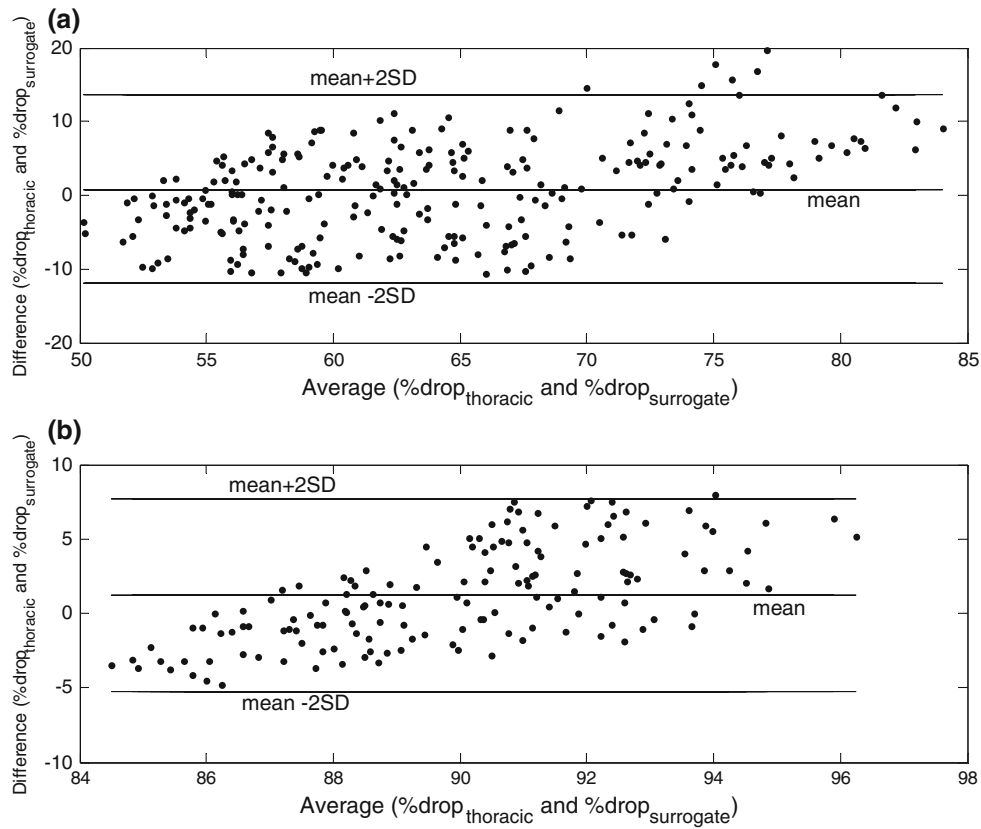


FIGURE 8. Bland–Altman plots of the relationship of the difference between % drop in thoracic signal and that in surrogate respiratory signals for 250 OSA events (a) and 150 CSA events (b) vs. their average value. Mean bias (—), +2SD and –2SD lines are shown. SD = standard deviation.

TABLE 3. OSA/CSA classification performance (overall accuracy, sensitivity, and specificity) on independent test set (80 OSA and 80 CSA) of RSA, EDR, and a combination of RSA, EDR and wavelet-EDR features using SVR.

RSA			EDR			Wavelet-EDR			SVR (RSA + EDR + wavelet-EDR)		
Sens (%)	Spec (%)	Acc (%)	Sens (%)	Spec (%)	Acc (%)	Sens (%)	Spec (%)	Acc (%)	Sens (%)	Spec (%)	Acc (%)
92.31	77.78	89.16	89.23	44.44	79.52	91.4	87.67	90.52	92.5	95	93.75

Acc, Accuracy; Sens, Sensitivity; Spec, Specificity. Sensitivity is for OSA detection accuracy and specificity is for CSA detection accuracy.

the performance criterion to select the best parameter set. Therefore data-intensive computational burden was significantly reduced. Parameter C determines the trade-off between the model complexity (flatness) and the degree to which deviations larger than ε are tolerated in optimization formulation (Eq. 1). For example, if C is too large (infinity), then the objective is to minimize the empirical risk only, without regard to model complexity part in the optimization formulation. Parameter ε controls the width of the ε -insensitive zone, used to fit the training data. The value of ε can affect the number of support vectors used to construct the regression function. The greater the ε , the fewer the support vectors that are selected. On the other hand,

greater ε -values result in more “flat” estimates. Hence, both C and ε -values affect model complexity (but in a different way).

In this study, the RIP was used as a gold standard of respiratory monitoring which measures the changes in the expansion and contraction of the thoracic and abdominal cavities. Placing an elastic belt in series with a piezo-electric sensor does this. One is placed at the level of the upper thorax, generally right underneath the arms to pick up rib-cage movements, and the other is placed at the level of the umbilicus to pick up abdominal movements. This study focused on ECG and SVR-based surrogate respiratory signal that can classify OSA and CSA events. The proposed algorithm

can be applied to recognize OSA or CSA types after the event is detected. For example, our earlier study¹⁰ can be used to detect individual apnea events. Although hypopneas were not used in this study, it may, however, be an interesting topic to look at how SVR can model respiratory movements during hypopneas. In future, esophageal catheter pressure signal which represents the respiratory effort (pressure) in sleep-disordered breathing could be attempted to use as a standard reference of respiratory signal to develop the model for surrogate respiratory effort signal in sleep-related breathing events. In addition to OSA/CSA discrimination, other potential application of our model may be to assess the severity of airway obstruction in patients with obstructive airway disease including asthma, bronchiolitis, and chronic obstructive pulmonary disease (COPD).

ACKNOWLEDGMENTS

The authors would like to thank members of the Sleep Research Team at the Institute of Breathing and Sleep at Austin Hospital, Melbourne for their assistance during sleep studies.

REFERENCES

- ¹American Academy of Sleep Medicine Task Force (AASM). Sleep-related breathing disorders in adults: recommendations for syndrome definition and measurement techniques in clinical research. *Sleep* 22:667–689, 1999.
- ²Bao, Y., and Z. Liu. A Fast Grid Search Method in Support Vector Regression Forecasting Time Series, Vol. 4224. LNCS, pp. 504–511, 2006.
- ³Bradley, T. D., and J. S. Floras. Sleep apnea, heart failure. Part I. Obstructive sleep apnea. *Circulation* 107:1671, 2003.
- ⁴Cherkassky, V., and Y. Ma. Practical selection of SVM parameters and noise estimation for SVM regression. *Neural Netw.* 17:113–126, 2004.
- ⁵Cortes, C., and V. Vapnik. Support vector networks. *Mach. Learn.* 20:273–297, 1995.
- ⁶Cysarz, D., R. Zerm, H. Bettermann, M. Frühwirth, M. Moser, and M. Kröz. Comparison of respiratory rates derived from heart rate variability, ECG amplitude, and nasal/oral airflow. *Ann. Biomed. Eng.* 36(12):2085–2094, 2008.
- ⁷Ferber, R., R. Millman, M. Coppola, *et al.* Portable recording in the assessment of obstructive sleep apnea. ASDA standards of practice. *Sleep* 17(4):378–392, 1994.
- ⁸Gunn, S. Support Vector Machines for Classification and Regression, ISIS Tech. Rep. Southampton, UK: Univ. Southampton, 1998.
- ⁹Khandoker, A. H. Regulation of Cardiac Rhythm in Avian Embryos and Hatchlings in Altered Environments. Ph.D. dissertation, Muroran Institute of Technology, Japan.
- ¹⁰Khandoker, A. H., J. Gubbi, and M. Palaniswami. Automated scoring of obstructive sleep apnea and hypopnea events using short term electrocardiogram recordings. *IEEE Trans. Inf. Technol. Biomed.* 13(6):1057–1067, 2009.
- ¹¹Khandoker, A. H., M. Palaniswami, and C. K. Karmakar. Support vector machines for automated recognition of obstructive sleep apnoea syndrome from electrocardiogram recordings. *IEEE Trans. Inf. Technol. Biomed. Eng.* 13(1): 37–48, 2009.
- ¹²Mazzanti, B., C. Lamberti, and J. de Bie. Validation of an ECG-derived respiration monitoring method. *Comput. Cardiol.* 30:613–616, 2003.
- ¹³Moody, G., R. Mark, A. Zoccola, and S. Mantero. Derivation of respiratory signals from multi-lead ECGs. *Comput. Cardiol.* 12:113–116, 1985.
- ¹⁴O'Brien, C., and C. Heneghan. A comparison of algorithms for estimation of a respiratory signal from the surface electrocardiogram. *Comput. Biol. Med.* 37:305–314, 2007.
- ¹⁵Penzel, T., J. McNames, P. de Chazal, B. Raymond, A. Murray, and G. Moody. Systematic comparison of different algorithms for apnoea detection based on electrocardiogram recordings. *Med. Biol. Eng. Comput.* 40: 402–407, 2002.
- ¹⁶Pinciroli, F., R. Rossi, and L. Vergani. Detection of electrical axis variation for the extraction of respiratory information. *Comput. Cardiol.* 12:499–502, 1985.
- ¹⁷Roche, F., J. M. Gaspoz, I. Court-Fortune, P. Minini, V. Pichot, D. Duverney, F. Costes, J. R. Lacour, and J. C. Barthélémy. Screening of obstructive sleep apnea syndrome by heart rate variability analysis. *Circulation* 100(13): 1411–1415, 1999.
- ¹⁸Roche, F., V. Pichot, E. Sforza, I. Court-Fortune, D. Duverney, F. Costes, M. Garet, and J. C. Barthélémy. Predicting sleep apnoea syndrome from heart period: a time-frequency wavelet analysis. *Eur. Respir. J.* 22(6): 937–942, 2003.
- ¹⁹Scholkopf, B., J. Burges, and A. Smola. *Advances in Kernel Methods: Support Vector Machine.* MIT Press, 1999.
- ²⁰Shineerson, J. M. *Sleep Medicine: A Guide to Sleep and Its Disorder.* Blackwell Publishing, pp. 230–231, 2005.
- ²¹Travaglini, A., C. Lamberti, J. DeBie, and M. Ferri. Respiratory signal derived from eight-lead ECG. *Comput. Cardiol.* 25:65–68, 1998.
- ²²Trikalinos, T. A., S. Ip, G. Raman, S. Cepeda, E. M. Balk, C. D'Ambrosio, and J. Lau. Home Diagnosis of Obstructive Sleep Apnea–Hypopnea Syndrome. Technology Assessment Program, Technical Report. Agency for Healthcare Research and Quality, 2007.
- ²³Vapnik, V. N. *The Nature of Statistical Learning Theory.* New York: Springer, 1995.
- ²⁴Wexler, L., D. H. Bergel, I. T. Gabe, G. S. Makin, and C. J. Mills. Velocity of blood flow in normal human venae cavae. *Circ. Res.* 23:349–359, 1968.